Inorganic Chemistry

Article

pubs.acs.org/IC

Relation between the Catalytic Efficiency of the Synthetic Analogues of Catechol Oxidase with Their Electrochemical Property in the Free State and Substrate-Bound State

Prateeti Chakraborty,[†] Jaydeep Adhikary,[†] Bipinbihari Ghosh,[∥] Ria Sanyal,[†] Shyamal Kumar Chattopadhyay,*[,∥] Antonio Bauzá,[‡] Antonio Frontera,*[,‡] Ennio Zangrando,*[,§] and Debasis Das*[,†]

[†]Department of Chemistry, University of Calcutta, 92 A. P. C. Road, Kolkata-700 009, India

[‡]Departament de Química, Universitat de les Illes Balears, Crta. De Valldemossa km 7.5, 07122 Palma, Baleares, Spain

[§]Dipartimento di Scienze Chimiche, University of Trieste, Via L. Giorgieri 1, 34127 Trieste, Italy

[∥]Department of Chemistry, Bengal Engineering and Science University, Howrah, India

Supporting Information

ABSTRACT: A library of 15 dicopper complexes as synthetic analogues of catechol oxidase has been synthesized with the aim to determine the relationship between the electrochemical behavior of the dicopper(II) species in the absence as well as in the presence of 3,5-di-*tert*-butylcatechol (3,5-DTBC) as model substrate and the catalytic activity, k_{cat}, in DMSO medium. The complexes have been characterized by routine physicochemical techniques as well as by X-ray single-crystal structure analysis in some cases. Fifteen "end-off" compartmental ligands have been designed as 1 + 2 Schiff-base condensation product of 2,6-diformyl-4-R-phenol (R = Me, ^{t}Bu, and Cl) and five different amines, *N*-(2-aminoethyl)-piperazine, *N*-(2-aminoethyl)pyrrolidine, *N*-(2-aminoethyl)-morpholine, *N*-(3-aminopropyl)morpholine, and *N*-(2-aminoethyl)piperidine. Interestingly, in case of the combination of 2,6-diformyl-4-methylphenol and *N*-(2-aminoethyl)morpholine/*N*-(3-aminopropyl)morpholine/*N*-(2-aminoethyl)piperidine 1 + 1 condensation becomes the reality and the ligands are denoted as $L2^{1-3}$. On reaction of copper(II) nitrate with $L2^{1-3}$ in situ complexes **3**, **12**, and **13** are formed having general formula $Cu_2(L2^{1-3})_2(NO_3)_2$. The remaining 12 ligands obtained as 1 + 2 condensation products are denoted as $L1^{1-12}$, which produce complexes having general formula $Cu_2(L1^{1-12})(NO_3)_2$. Catecholase activity of all 15 complexes has been investigated in DMSO medium using 3,5-DTBC as model substrate. Treatment on the basis of Michaelis−Menten model has been applied for kinetic study, and thereby turnover number, k_{cat}, values have been evaluated. Cyclic voltametric (CV) and differential pulse voltametric (DPV) studies of the complexes in the presence as well as in the absence of 3,5-DTBC have been thoroughly investigated in DMSO medium. From those studies it is evident that oxidation of 3,5-DTBC catalyzed by dicopper(II) complexes proceed via two steps: first, semibenzoquinone followed by benzoquinone with concomitant reduction of Cu^{II} to Cu^{I}. Our study reveals that apparently there is nearly no linear relationship between k_{cat} and $E°$ values of the complexes. However, a detailed density functional theory (DFT) calculation sheds light on this subject. A very good correlation prevails in terms of the energetics associated with the Cu^{II} to Cu^{I} reduction process and k_{cat} values, as revealed from the combined theoretical and experimental approach.

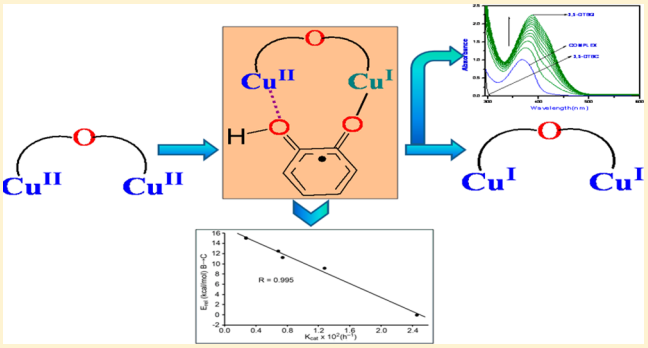

INTRODUCTION

Catechol oxidase (CO), the less well-known member of the type-3 copper proteins, found in plant tissues and crustaceans, catalyzes the oxidation of a wide range of *o*-diphenols (catechols) to the corresponding *o*-quinones, a process known as catecholase activity (Scheme 1).[1−3] The *o*-quinones are highly reactive compounds and readily undergo an autopolymerization leading to formation of melanin, a brown polyphenolic pigment, thought to protect damaged tissues against pathogens or insects.[1] The catechol to quinone conversion is of great importance in medical diagnosis for determination of the hormonally active catecholamines adrenaline, noradrenaline, and dopa.[4]

Studies on the synthetic analogues of catechol oxidase have become an emerging field of modern research in bioinorganic chemistry to understand the in-depth functional mechanisms of catechol oxidase and elucidate different internal and external

Received: March 5, 2014
Published: July 29, 2014

   dx.doi.org/10.1021/ic5005177 | *Inorg. Chem.* 2014, 53, 8257−8269

Scheme 1. Reaction Pathway of the Oxygenation and Oxidation Catalyzed by TYR and CO

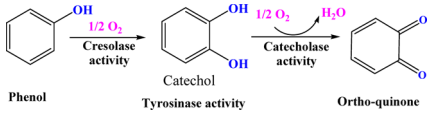

factors which may influence the activity.[1−3,5−18] It is now well documented that among the external factors, the most important contributors are the pH of the medium, the nature of the model substrate, and the nature of the solvent. As far as internal factors are concerned the dominating effects come from the Cu−Cu distance, the flexibility of the coordinating ligands, and the coordination environment of the copper centers. Recently, it was documented that the presence of a positive charge center close to the metal center(s) may enhance the activity. Oxidation of catechol to quinone is a two-electron oxidation process. Most of the researchers working in elucidating the mechanistic pathway involved in catecholase activity believe that metal-centered redox participation, i.e., reduction of Cu^{II} to Cu^{I}, is the key step responsible for oxidation of catechol, although a radical pathway is now emerging to be a reasonable alternative, at least for nickel and zinc systems.[19] However, since redox participation of two copper centers appears to be crucial in catecholase activity, the electrochemical behavior of the synthetic analogues of CO could clarify the mechanism of their catecholase activity. Surprisingly, only a few scattered reports are in the literature[5,9,20−24] where this particular issue has been pointed out. Krebs et al., in one of their classical papers,[1] after thorough electrochemical analysis came to the conclusion that the poorly defined redox chemistry of their Mannich base dicopper complexes could not allow them to establish any relationship between the electrochemical properties of the complexes and the oxidation potential of the model substrate, 3,5-di-*tert*-butylcatechol (3,5-DTBC). However, Neves et al.[10] observed a very good correlation between $(\Delta E)_{1,2}$ (= $E(\mathrm{red})_1 - E(\mathrm{red})_2$) and kinetic parameter k_2 (second-order rate constant = k_{cat}/K_M) in their dinuclear Cu(II) complexes, although they failed to find any correlation between k_{cat}/K_M and the individual $E(\mathrm{red})_1$ and $E(\mathrm{red})_2$ of the complexes.

In order to get a better understanding on this intriguing issue we planned to investigate the electrochemical property and catecholase activity of as many as 15 closely related dicopper(II) complexes in DMSO medium extensively. To fulfill our purpose we designed 15 "end-off" compartmental ligands as 1 + 2 the Schiff-base condensation product of 2,6-diformyl-4-R-phenol (R= Me, ^{t}Bu and Cl) and five different amines, *N*-(2-aminoethyl)piperazine, *N*-(2-aminoethyl)-pyrrolidine, *N*-(2-aminoethyl)morpholine, *N*-(3-aminopropyl)-morpholine, and *N*-(2-aminoethyl)piperidine (Scheme 2). In three cases, instead of 1 + 2 condensation, 1 + 1 condensation becomes a reality. In those cases the diformyl species is 2,6-diformyl-4-methylphenol and amines are *N*-(2-aminoethyl)-piperidine. *N*-(2-Aminoethyl)morpholine and *N*-(3-aminopropyl)morpholine and the ligands are denoted as $L2^{1-3}$. On reaction of copper(II) nitrate with $L2^{1-3}$ in situ complexes **3**, **12**, and **13** are generated having general formula $Cu_2(L2^{1-3})_2(NO_3)_2$. The remaining 12 ligands obtained as 1 + 2 condensation products are denoted as $L1^{1-12}$ which produce complexes **1**, **2**, **4**−**11**, **14**, and **15** having general formula $Cu_2(L1^{1-12})(NO_3)_2$. Catecholase activity of all 15 complexes

Scheme 2. Structure and Labels of Synthesized Compartmental Ligands

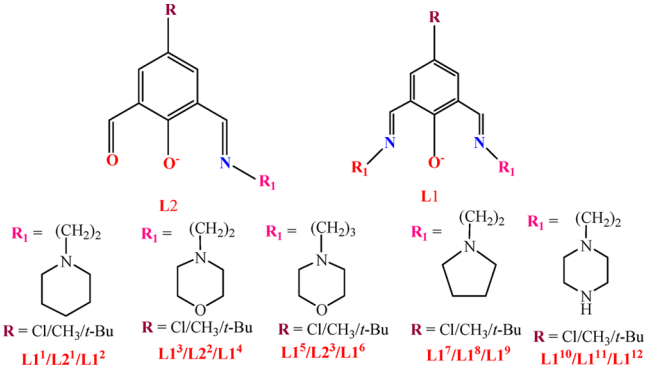

has been investigated in DMSO medium using 3,5-DTBC as model substrate. Cyclic voltametric (CV) and differential pulse voltametric (DPV) studies of the complexes in the presence as well as in the absence of 3,5-DTBC have been thoroughly investigated in DMSO medium. A detailed DFT calculation has been performed to make a breakthrough on this subject. Although no linear relationship has apparently been established between E° and k_{cat} values, a very good correlation prevails in terms of the energetics associated with the electrochemical behavior of the catechol-bound dicopper(II) system involved in the catalytic process and k_{cat} values, as revealed from the combined theoretical and experimental approach. All those interesting findings are vividly portrayed in this article.

EXPERIMENTAL SECTION

Physical Methods and Materials. Elemental analyses (carbon, hydrogen, and nitrogen) were performed using a Perkin−Elmer 240C elemental analyzer, and copper content was estimated gravimetrically. Infrared spectra were recorded on KBr disks (400−4000 cm^{-1}) with a Perkin−Elmer RXI FTIR spectrophotometer. Electronic spectra (200−800 nm) were measured at room temperature on a Shimadzu UV-3101PC using dry acetonitrile/dry methanol/nujol as medium. Cyclic voltammetric and DPV measurements were performed using a CH1106A potentiostat with glassy carbon (GC) as the working electrode, Pt wire as the counter electrode, and Ag,AgCl/sat KCl as the reference electrode. All solutions were purged with dinitrogen prior to measurements.

High-purity *N*-(2-aminoethyl)piperazine, *N*-(2-aminoethyl)-pyrrolidine, *N*-(2-aminoethyl)morpholine, *N*-(3-aminopropyl)-morpholine, and *N*-(2-aminoethyl)piperidine were purchased from commercial sources (Fluka, Lancaster Chemical Co. Inc., Aldrich) and used as received. The 2,6-diformyl-4-R-phenols (R = methyl, *tert*-butyl, chloro) were prepared according to the literature method.[25] Solvents were dried according to standard procedures and distilled prior to use. All other chemicals used were of AR grade.

Synthesis of the Complexes. The following general template synthetic route was adopted for preparing all complexes. A methanolic solution of copper nitrate was added to the ligand solution formed in situ via condensation of 2,6-diformyl-4-R-phenol (where R= methyl, *tert*-butyl, and chloro) with the corresponding amines maintaining the same molar ratio. The preparation, composition, and other physicochemical characteristics of all complexes using the template technique are given below.

Syntheses. *a. $[Cu_2(L1^1)(OH)(H_2O)(NO_3)_2]$, **1**.* To a methanolic solution (5 mL) of *N*-(2-aminoethyl)piperidine (0.256 g, 2 mmol) a methanolic solution (10 mL) of 4-chloro-2,6-diformylphenol (0.180 g, 1 mmol) was added in a dropwise manner, and the mixture was refluxed 30 min. Then a methanolic solution (15 mL) of copper nitrate (0.604 g, 2.5 mmol) was added to it, and the resulting mixture was allowed to reflux for 2 h. The deep green solution was filtered and

dx.doi.org/10.1021/ic5005177 | Inorg. Chem. 2014, 53, 8257−8269

Table 1. Crystallographic Data and Details of Refinements for Complexes 1−3 and 8−10[a]

	1·H_2O	2·H_2O	3·2H_2O	8	9·H_2O	10·2H_2O
empirical formula	$C_{22}H_{35}ClCu_2N_6O_9$	$C_{26}H_{44}Cu_2N_6O_9$	$C_{32}H_{50}Cu_2N_8O_{20}$	$C_{20}H_{33}ClCu_2N_6O_{10}$	$C_{48}H_{40}Cu_4N_{12}O_{18}$	$C_{20}H_{39}ClCu_2N_{10}O_{17}$
M	690.09	711.75	993.88	680.05	1367.40	854.14
cryst syst	triclinic	monoclinic	triclinic	monoclinic	tetragonal	orthorhombic
space group	$P\bar{1}$	$P2_1/n$	$P\bar{1}$	$P2_1/m$	$P4_2/n$	$Pna2_1$
a/Å	9.531(6)	15.907(3)	10.059(3)	8.1106(3)	24.820(3)	8.7183(5)
b/Å	12.534(6)	11.836(2)	10.470(3)	12.3324(5)		40.122(3)
c/Å	13.472(7)	17.008(3)	11.463(4)	13.7055(5)	10.501(2)	9.5437(6)
α/deg	100.526(5)		77.391(3)			
β/deg	103.720(5)	94.178(2)	89.205(3)	102.507(2)		
γ/deg	106.472(4)		66.130(3)			
V/Å^3	1444.3(13)	3193.5(10)	1073.6(6)	1338.34(9)	6469.0(18)	3338.3(4)
Z	2	4	1	2	4	4
D_{calcd}/g cm^{-3}	1.587	1.480	1.537	1.688	1.404	1.699
μ/mm^{-1}	1.623	1.390	1.077	1.753	1.369	1.443
$F(000)$	712	1488	516	684	2848	1760
total data	7223	21837	7278	24430	24566	33586
unique data	4207	5720	3993	7253	4543	5005
R_{int}	0.0510	0.0348	0.0284	0.0358	0.0667	0.1276
reflns $I > 2\sigma(I)$	2450	4446	2599	5172	2455	3588
params	388	403	300	218	427	472
goodness-of-fit	1.094	1.051	1.039	1.015	1.167	0.951
R_1	0.0757	0.0519	0.0756	0.0445	0.0703	0.0488
wR_2 $(I > 2\sigma(I))^b$	0.1462	0.1594	0.2114	0.1126	0.2241	0.0967
residuals/e Å^{-3}	0.767, −0.710	1.249, −0.401	1.367, −0.525	0.685, −0. 964	0.744, −0.355	0.492, −0.271

[a]CCDC 988842−988847 contain the supplementary crystallographic data for this paper. These data can be obtained free charge from the Cambridge Crystallographic Data Centre via http://www.ccdc.cam.ac.uk/5datarequest/cif. [b]$R1 = \Sigma||F_o| - |F_c||/\Sigma|F_o|$, $wR2 = [\Sigma w (F_o^2 - F_c^2)^2/\Sigma w (F_o^2)^2]^{1/2}$.

kept in a $CaCl_2$ desiccator. Deep green crystals suitable for X-ray data collection were obtained from the filtrate after a few days (yield 75%). Anal. Calcd for $C_{23}H_{33}ClCu_2N_5O_9$: C, 31.90; H, 3.81; N, 8.08. Found: C, 31.87; H, 3.86; N, 7.99. IR (KBr): ν(C═N) 1651 cm^{-1}; ν(skeletal vibration) 1552 cm^{-1}; ν(H_2O) 3413 cm^{-1}; ν(NO_3^-) 1384 cm^{-1}.

*b. [Cu_2(L1^2)(OH)(H_2O)(NO_3)$_2$], **2**.* **2** was prepared by adopting the same procedure as in the case of **1** using 4-*tert*-butyl-2,6-diformylphenol (0.206 g, 1 mmol) instead of 4-chloro-2,6-diformylphenol. Deep green colored single crystals suitable for X-ray data collection were obtained from the filtrate after a week (yield 65%). Anal. Calcd for $C_{26}H_{44}Cu_2N_6O_9$: C, 43.83; H, 6.18; N, 11.98. Found: C, 43.75; H, 6.10; N, 11. 9. IR (KBr): ν(C═N) 1639 cm^{-1}; ν(skeletal vibration) 1550 cm^{-1}; ν(H_2O) 3435 cm^{-1}; ν(NO_3^-) 1384 cm^{-1}.

*c. [Cu(L2^1)(H_2O)(NO_3)]$_2$, **3**.* **3** was prepared following the same procedure as for **1** using 4-methyl-2,6-diformylphenol (0.184 g, 1 mmol) instead of 4-chloro-2,6-diformylphenol. Single crystals suitable for diffraction were obtained from the filtrate after 2 days (yield 80%). Anal. Calcd for $C_{32}H_{50}Cu_2N_8O_{20}$: C, 38.62; H, 5.03; N, 11.40. Found: C, 38.63; H, 5.09; N, 11.26. IR (KBr): ν(C═O) 1680 cm^{-1}; ν(C═N) 1653 cm^{-1}; ν(skeletal vibration) 1552 cm^{-1}; ν(H_2O) 3429 cm^{-1}; ν(NO_3^-) 1383 cm^{-1}.

*d. [Cu_2(L1^3)(OH)(H_2O)(NO_3)$_2$], **4**.* **4** was prepared following the same procedure as for **1** just using *N*-(2-aminoethyl) morpholine (0.130 g,1 mmol) in place of *N*-(2-aminoethyl)piperidine. A deep green colored solid mass was obtained from the filtrate after a few days on keeping the filtrate at room temperature (yield 80%.) Anal. Calcd for $C_{20}H_{31}ClCu_2N_6O_{11}$: C, 34.65; H, 4.47; N, 12.13. Found: C, 34.54; H, 4.58; N, 12.19. IR (KBr): ν(C═N) 1650 cm^{-1}; ν(skeletal vibration) 1552 cm^{-1}; ν(H_2O) 3436 cm^{-1}; ν(NO_3^-) 1384 cm^{-1}.

*e. [Cu_2(L1^4)(OH)(H_2O)(NO_3)$_2$], **5**.* **5** was prepared adopting the same procedure as for **2** by replacing *N*-(2-aminoethyl) piperidine with *N*-(2-aminoethyl) morpholine (0.130 g, 1 mmol). Deep green colored single crystals suitable for X-ray data collection were obtained from the filtrate after a week on keeping the filtrate in a $CaCl_2$ desiccator (yield 80%). Anal. Calcd for $C_{24}H_{40}Cu_2N_6O_{11}$: C, 40.33; H, 5.60; N, 11.76. Found: C, 40.24; H, 5.66; N, 11.69. IR (KBr): ν(C═N) 1636 cm^{-1}; ν(skeletal vibration) 1553 cm^{-1}; ν(H_2O) 3435 cm^{-1}; ν(NO_3^-) 1384 cm^{-1}.

*f. [Cu_2(L1^5)(OH)(H_2O)(NO_3)$_2$], **6**.* **6** was prepared adopting the same procedure as for **4** using *N*-(2-aminopropyl) morpholine (0.144g, 1 mmol) instead of *N*-(2-aminoethyl) morpholine. A deep green colored crystalline solid mass was obtained from the filtrate after a few days (yield 80%). Anal. Calcd for $C_{22}H_{35}$ $ClCu_2N_6O_{11}$: C, 36.64; H, 4.85; N, 11.65. Found: C, 36.69; H, 4.69; N, 11.69. IR (KBr): ν(C═N) 1643 cm^{-1}; ν(skeletal vibration) 1550 cm^{-1}; ν(H_2O) 3413 cm^{-1}; ν(NO_3^-) 1384 cm^{-1}.

*g. [Cu_2(L1^6)(OH)(H_2O)(NO_3)$_2$], **7**.* **7** was prepared following the same procedure as for **5** using *N*-(2-aminopropyl)morpholine (0.144g, 1 mmol) instead of *N*-(2-aminoethyl)morpholine. Deep green colored single crystals suitable for X-ray data collection were obtained from the filtrate after a week on keeping the filtrate in a $CaCl_2$ desiccator (yield 80%). Anal. Calcd for $C_{26}H_{44}Cu_2N_6O_{11}$: C, 42.04; H, 4.71; N, 11.32. Found: C, 42.14; H, 4.65; N, 11.39. IR (KBr): ν(C═N) 1642 cm^{-1}; ν(skeletal vibration) 1551 cm^{-1}; ν(H_2O) 3434 cm^{-1}; ν(NO_3^-) 1384 cm^{-1}.

*h. [Cu_2(L1^7)(OH)(H_2O)$_2$(NO_3)$_2$], **8**.* **8** was prepared following the same procedure as for **1** using *N*-(2-aminoethyl)pyrrolidine (0.114g, 1 mmol) instead of *N*-(2-aminoethyl)piperidine. Crystals suitable for X-ray diffraction were obtained from the filtrate after 2 days on keeping the filtrate at room temperature (yield 80%). Anal. Calcd for $C_{20}H_{33}ClCu_2N_6O_{10}$: C, 35.21; H, 4.86; N, 12.4. Found: C, 35.29; H, 4.76; N, (12.35. IR (KBr): ν(C═N) 1650 cm^{-1}; ν(skeletal vibration) 1551 cm^{-1}; ν(H_2O) 3435 cm^{-1}; ν(NO_3^-) 1384 cm^{-1}.

*I. [Cu_2(L1^9)(OH)(H_2O)(NO_3)$_2$], **9**.* **9** was prepared following the same procedure as for **2** using *N*-(2-aminoethyl)pyrrolidine (0.114g, 1 mmol) instead of *N*-(2-aminoethyl)piperidine. Crystals suitable for X-ray diffraction were obtained from the filtrate after several days on keeping the filtrate in a $CaCl_2$ desiccator. A deep green colored solid mass was obtained from the filtrate after a few days on keeping the filtrate at room temperature (yield 80%). Anal. Calcd for $C_{24}H_{39}Cu_2N_6O_9$: C, 42.18; H, 5.71; N, 12.30. Found: C, 42.14; H,

dx.doi.org/10.1021/ic5005177 | Inorg. Chem. 2014, 53, 8257−8269

5.68; N, 12.39. IR (KBr): ν(C=N) 1644 cm^{-1}; ν(skeletal vibration) 1552 cm^{-1}; $\nu(H_2O)$ 3422 cm^{-1}; $\nu(NO_3^-)$ 1371 cm^{-1}.

j. $[Cu_2(H_2L1^{10})(OH)(H_2O)(NO_3)_4]$, ***10***. **10** was prepared following the same procedure as **4** using *N*-(2-aminoethyl) piperazine (0.129g, 1 mmol) instead of *N*-(2-aminoethyl)morpholine. Single crystals suitable for diffraction were obtained after a week from the filtrate kept in a $CaCl_2$ desiccator (yield 80%). Anal. Calcd for $C_{20}H_{39}ClCu_2N_{10}O_{17}$: C, 28.12; H, 4.6; N, 16.4. Found: C, 28.09; H, 4.56; N, 16.39. IR (KBr): ν(C=N) 1647 cm^{-1}; ν(skeletal vibration) 1551 cm^{-1}; $\nu(H_2O)$ 3419 cm^{-1}; $\nu(NO_3^-)$ 1368 cm^{-1}.

k. $[Cu_2(L1^{12})(OH)(H_2O)(NO_3)_2]$, ***11***. **11** was prepared following the same procedure like **8** using 4-*tert*-butyl-2,6-diformylphenol (0.206 g, 1 mmol) instead of 4-chloro-2,6-diformylphenol. Deep green colored crystals were obtained from the filtrate after a few days on keeping the filtrate at room temperature (yield 80%). Anal. Calcd for $C_{24}H_{48}Cu_2N_{10}O_{17}$: C, 32.95; H, 5.49; N, 16.01. Found: C, 32.88; H, 5.6; N, 15.89. IR (KBr): ν(C=N) 1645 cm^{-1}; ν(skeletal vibration) 1549 cm^{-1}; $\nu(H_2O)$ 3413 cm^{-1}; $\nu(NO_3^-)$ 1384 cm^{-1}.

Complexes **12**−**15** of composition $[Cu(HL2^2)(H_2O)(NO_3)]_2(NO_3)_2{\cdot}2H_2O$, $[Cu(L2^3)(H_2O)(NO_3)]_2$, $[Cu_2(L1^8)(OH)(H_2O)_2](NO_3)_2$, and $[Cu_2(H_2L1^{11})(OH)(H_2O)(NO_3)](NO_3)_3{\cdot}2H_2O$ were prepared by following the method previously reported by us.[18]

X-ray Data Collection and Crystal Structure Determinations. Data collection of the structures reported was carried out on a Bruker Smart CCD diffractometer equipped with graphite-monochromated Mo Kα radiation (λ = 0.71073 Å) at room temperature. Cell refinement, indexing, and scaling of the data set were carried out using Bruker Smart Apex and Bruker Saint packages.[26] Structures were solved by direct methods and subsequent Fourier analyses[27] and refined by the full-matrix least-squares method based on F^2 with all observed reflections.[27] In **1** a nitrate anion is disordered over two positions at half occupancy with an oxygen atom (O8 and O11) sharing the same site with a water molecule (O1w and O2w, respectively, with occupancy = 0.5). In **2** two residuals in the difference Fourier map were treated as lattice water molecules at half occupancy (H atoms not located). In **3** the piperidine ring and a nitrate anion were found disordered over two positions (occupancies of 0.57/0.43 and 0.76/0.24, respectively); thus, the piperidine carbon atoms were isotropically refined. In **8** the uncoordinated nitrate anion was found disordered over two positions: one having all atoms and the second only the nitrogen and one oxygen sitting in a crystallographic symmetry plane. The crystal of **9** was low diffracting due to the disorder over two positions observed in the *tert*-butyl group and in the methylene groups attached at N3 and N4 (occupancies of 0.64/0.36, 0.63/37, and 0.64/0.36). Moreover, beside nitrate N3, located on a center of symmetry, to nitrate N7 an occupancy of 0.50 was assigned for the sake of neutrality. Non-hydrogen atoms were anisotropically refined except the *tert*-butyl in complex **9**. All calculations were performed using WinGX System, Ver 1.80.05.[28] Pertinent crystallographic data and refinement details are summarized in Table 1.

Theoretical Methods. Energies of all complexes included in this study were computed at the BP86-D3/def2-TZVPD level of theory using the optimized geometries within the program TURBOMOLE version 6.4.[29] Solvent effects were evaluated using the COSMO (Conductor like Screening Model) solvation model.[30] For the calculations we used the BP86 functional with the latest available correction for dispersion (D3).

RESULTS AND DISCUSSION

Four structurally characterized copper(II) complexes (**12**−**15**) were prepared by adopting the template synthesis technique and identified by their reported physicochemical properties.[18] The 11 new complexes, namely, complexes **1**−**11**, were synthesized by treating a methanolic solution of copper(II) nitrate trihydrate with the Schiff base formed in situ between 2,6-diformyl-4-R-phenol (where R= *tert*-butyl, chloro, methyl) and the diamines. In some cases single crystals suitable for X-ray analysis were obtained. FT-IR spectral study reveals that all complexes exhibit bands due to the C=N stretch in the range 1630−1648 cm^{-1} and skeletal vibration in the range 1545−1555 cm^{-1}. The presence of weakly coordinated NO_3^- anion in all complexes is indicated by the broad band centered in the range 1365−1385 cm^{-1}.[31] Electronic spectra of all complexes studied in DMSO medium display very similar absorption bands in the range 370−415 and 640−650 nm. The observed lower energy band may be assigned due to the d−d transition, and the corresponding strong higher energy single band (between 370 and 415 nm) is due to combination of both phenoxido−Cu(II) and hydroxido−Cu(II) LMCT bands. It is well known that for a d^9 system the electronic transition $^2E_g \rightarrow {}^2T_{2g}$ is expected to take place at around 800 nm for octahedral coordination geometry, and this band undergoes a significant blue shift for octahedral distortions to square-pyramidal and square-planar structures.[32] In all complexes the d−d transition positions are in agreement with a square-pyramidal geometry around the metal centers.

Description of Crystal Structures. Structural analysis of complexes **1**, **2**, **8**, **9**, and **10** reveals for all a $[Cu_2(L1)(OH)]$ unit with metals chelated by the pentacoordinating ligand L1 and bridged by a hydroxido oxygen. In each case the copper atoms complete their square planar coordination sphere through nitrate anions or aqua ligands. ORTEP drawings of complexes **1**, **8**, and **9** are shown in Figures 1−3; those of **2** and **10** are given in Figures S12 and S13, Supporting Information.

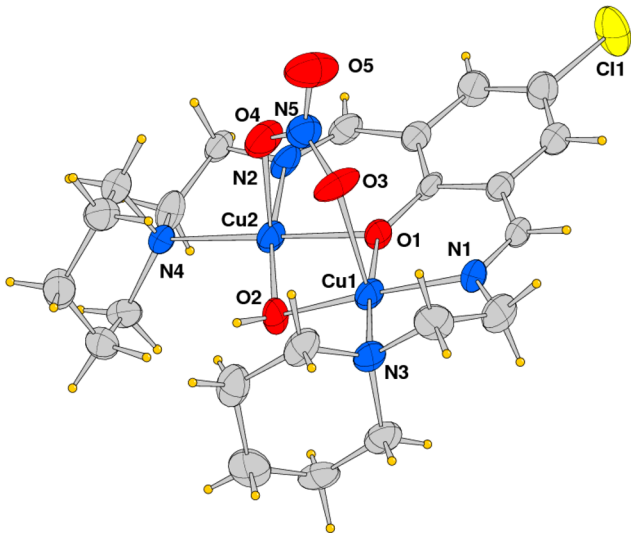

Figure 1. ORTEP drawing of the complex cation of complex **1**.

Complexes **1** and **2** show a close comparable metal coordination environment and differ only for the R group at the Schiff base (Cl and *t*Bu, respectively). Copper(II) atoms are chelated by the phenoxido oxygen, the imino and amino piperidine nitrogens of the ligand, and by a bridging hydroxide, completing the coordination sphere by a nitrate anion that acts as a bridging species toward the metals. In both complexes the basal Cu−O distances are comparable in lengths ranging from 1.897(3) to 2.006(7) Å (Table 2), showing a shorter value for the hydroxido oxygen. On the other hand, the Cu−N(imino) bond distances (range 1.919(4)−1.959(9) Å) are shorter than those involving the amino nitrogen of the heterocycle ring, falling between 2.036(4) and 2.097(8) Å) Å. The Cu−O(nitrate) distance at the apical position of the square planar

dx.doi.org/10.1021/ic5005177 | *Inorg. Chem.* 2014, 53, 8257−8269

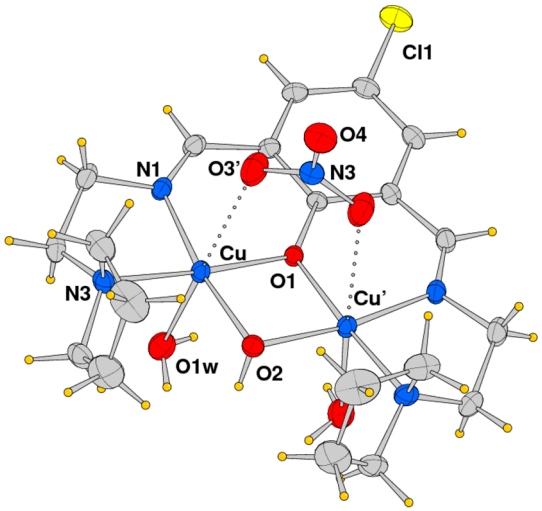

Figure 2. ORTEP drawing of the complex cation of complex **8** located on the crystallographic symmetry plane.

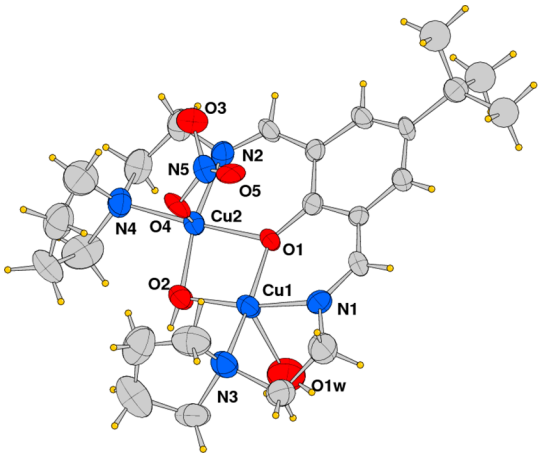

Figure 3. ORTEP drawing of the complex cation of complex **9**.

coordination geometry is sensibly longer falling in a range from 2.360(8) to 2.437(9) Å. The Cu(1)−O(1)−Cu(2) bond angle is ca. 95.3°, whereas the Cu(1)−O(2)−Cu(2) one, subtended by the hydroxido group, is slightly larger with an average value of 99.7°, leading to a metal−metal separation of 2.944(2) and 2.9049(8) Å in **1** and **2**, respectively.

The metal coordination environment of complexes **9** and **10** comprises the phenoxido oxygen and the imine- and amine-nitrogen donors, the bridging hydroxo group, and the square pyramidal geometry is completed by a monocoordinated nitrate and an aqua ligand on opposite side of the Schiff base ligand plane. Bond distances follow the trend observed for complexes **1** and **2** and typical for these types of dicompartmental copper species. A slight difference is detected between the Cu−N(pyrrolidine) bond lengths in complex **9** of 2.043(12) and 2.007(12) Å with respect to the Cu−N(piperazine) ones of 2.113(6) and 2.083(6) Å in **10**, Table 3. In complex **9** the nitrate N5 is located on a crystallographic inversion center, and it appears disordered, connecting two symmetry related complexes (Figure S14, Supporting Information).

In complex **10** the piperazine moieties, which attain a chair conformation, are protonated at the amine nitrogens leading to a tricationic complex species. This feature is confirmed by the number of nitrate counteranions and the NH_2 groups which

Table 2. Coordination Bond Lengths (Angstroms) and Angles (degrees) for Complexes 1 and 2

	1	2
Cu(1)−O(1)	2.006(7)	1.961(3)
Cu(1)−O(2)	1.925(6)	1.897(3)
Cu(1)−N(1)	1.951(8)	1.928(4)
Cu(1)−N(3)	2.097(8)	2.037(4)
Cu(1)−O(3)	2.360(8)	2.434(3)
Cu(2)−O(1)	1.980(6)	1.970(3)
Cu(2)−O(2)	1.937(7)	1.896(3)
Cu(2)−N(2)	1.959(9)	1.919(4)
Cu(2)−N(4)	2.075(7)	2.036(4)
Cu(2)−O(4)	2.437(9)	2.413(3)
Cu(1)−Cu(2)	2.944(2)	2.9049(8)
O(2)−Cu(1)−N(1)	167.6(3)	165.85(16)
O(2)−Cu(1)−O(1)	80.7(3)	79.69(12)
N(1)−Cu(1)−O(1)	90.0(3)	90.08(14)
O(2)−Cu(1)−N(3)	103.9(3)	103.25(13)
N(1)−Cu(1)−N(3)	85.4(4)	86.17(15)
O(1)−Cu(1)−N(3)	175.4(3)	174.41(13)
O(2)−Cu(1)−O(3)	97.2(3)	94.20(14)
N(1)−Cu(1)−O(3)	90.4(3)	95.40(16)
O(1)−Cu(1)−O(3)	87.4(3)	89.12(12)
N(3)−Cu(1)−O(3)	92.9(3)	95.37(13)
O(2)−Cu(2)−N(2)	170.6(3)	165.44(16)
O(2)−Cu(2)−O(1)	81.0(3)	79.52(12)
N(2)−Cu(2)−O(1)	90.6(3)	89.86(14)
O(2)−Cu(2)−N(4)	102.2(3)	103.40(13)
N(2)−Cu(2)−N(4)	85.9(3)	86.54(15)
O(1)−Cu(2)−N(4)	175.0(3)	175.03(13)
O(2)−Cu(2)−O(4)	93.3(3)	95.54(13)
N(2)−Cu(2)−O(4)	89.8(3)	94.28(15)
O(1)−Cu(2)−O(4)	83.1(3)	89.46(12)
N(4)−Cu(2)−O(4)	100.4(3)	94.22(13)

behave as H-bond donors toward nitrate oxygens and a lattice water molecule (N···O distance of 2.99−3.03 Å). The intermetallic distance in complex **9** is 2.934(2) Å, while in **10** it is 2.9596(11) Å, which is the longest among those here reported.

Complex **8** is located on a crystallographic symmetry plane passing in between the metals and referring the two halves of the phenolato ligand. The crystal structure shows that the equatorial plane of copper atoms is realized by doubly bridging phenoxido and hydroxido oxygen atoms and by the imine- and amine-nitrogen donors from L1[7] and from the pyrrolidine ring. The coordination sphere of the crystallographically independent copper ion is completed at axial sites by a water molecule (Cu−O1w = 2.5495(16) Å) and by a nitrate oxygen (Cu−O3′) at 2.7669(18) Å, indicating a weaker interaction and providing a pseudo-octahedral geometry as a consequence of the Jahn−Teller effect. The basal Cu−O distances are 1.9063(10) and 1.9726(9) Å (Table 4), the shorter value being relative to the hydroxido oxygen. On the other hand, the Cu−N(imino) bond distance (1.9393(13) Å) is slightly shorter than that involving the amino nitrogen of the heterocycle ring 2.0278(13) Å. The piperazine moieties attain a chair conformation. The bridging oxygen atoms locate the metals separated by 2.9450(4) Å.

Complexes **12** and **13** built with the methyl-phenolato moiety, already reported by us,[18] will not be described as they are isomorphous and isostructural with chloro derivative complexes **10** and **8**, respectively. X-ray structural data of all

dx.doi.org/10.1021/ic5005177 | Inorg. Chem. 2014, 53, 8257−8269

Table 3. Coordination Bond Lengths (Angstroms) and Angles (degrees) for Complexes 9 and 10

	9	10
Cu(1)−O(1)	1.977(9)	1.979(4)
Cu(1)−O(2)	1.933(10)	1.929(5)
Cu(1)−N(1)	1.932(11)	1.931(6)
Cu(1)−N(3)	2.043(12)	2.113(6)
Cu(1)−O(1w)	2.393(14)	2.305(6)
Cu(2)−O(1)	1.973(9)	1.972(5)
Cu(2)−O(2)	1.918(10)	1.919(5)
Cu(2)−N(2)	1.934(11)	1.919(6)
Cu(2)−N(4)	2.007(12)	2.083(6)
Cu(2)−O(4)	2.38(3)	2.398(6)
Cu(1)−Cu(2)	2.934(2)	2.9596(11)
O(2)−Cu(1)−N(1)	170.8(5)	170.0(2)
O(2)−Cu(1)−O(1)	80.6(4)	80.4(2)
N(1)−Cu(1)−O(1)	90.7(5)	90.7(2)
O(2)−Cu(1)−N(3)	102.8(5)	103.3(2)
N(1)−Cu(1)−N(3)	85.2(5)	84.7(3)
O(1)−Cu(1)−N(3)	168.9(5)	169.5(2)
O(1)−Cu(1)−O(1w)	96.6(4)	90.9(2)
O(2)−Cu(1)−O(1w)	92.4(4)	89.7(2)
N(1)−Cu(1)−O(1w)	91.6(5)	95.0(2)
N(3)−Cu(1)−O(1w)	93.9(5)	98.9(2)
N(2)−Cu(2)−O(2)	168.0(5)	169.1(2)
N(2)−Cu(2)−O(1)	89.7(4)	90.3(2)
O(2)−Cu(2)−O(1)	81.1(4)	80.80(18)
N(2)−Cu(2)−N(4)	85.7(5)	85.9(2)
O(2)−Cu(2)−N(4)	103.2(5)	102.4(2)
O(1)−Cu(2)−N(4)	174.8(4)	173.2(2)
N(2)−Cu(2)−O(4)	108.7(6)	92.5(2)
O(2)−Cu(2)−O(4)	77.2(6)	93.5(2)
O(1)−Cu(2)−O(4)	79.5(8)	88.4(2)
N(4)−Cu(2)−O(4)	104.3(8)	97.4(2)

Table 4. Coordination Bond Lengths (Angstroms) and Angles (degrees) for Complex 8[a]

Cu−O(1)	1.9726(9)	Cu−N(3)	2.0278(13)
Cu−O(2)	1.9063(10)	Cu−O(1w)	2.5495(16)
Cu−N(1)	1.9393(13)	Cu−O(3)′	2.7669(18)
		Cu−Cu′	2.9450(4)
O(2)−Cu−N(1)	170.89(5)	O(1w)−Cu−O(1)	89.80(6)
O(2)−Cu−O(1)	80.81(5)	O(1w)−Cu−O(2)	95.20(6)
N(1)−Cu−O(1)	90.84(5)	O(1w)−Cu−N(1)	88.37(6)
O(2)−Cu−N(3)	102.27(6)	O(1w)−Cu−N(3)	91.77(5)
N(1)−Cu−N(3)	85.96(6)	O(1w)−Cu−O(3)′	166.46(6)
		O(1)−Cu−N(3)	176.40(5)

[a]Primed atoms at x, $-y + 1/2$, z.

these complexes do not indicate any significant effect of the group in the para position of the phenolato ligand (Cl, Me, and *t*-Bu) on the coordination distances and on the intermetallic separation, and the slight differences observed may be attributed to a packing effect and to a lesser extent to H bonds realized in the crystal structure.

Different from previous complexes, the crystal structure of complex **3** reveals that it comprises a dinuclear complex cation located on a crystallographic inversion center, beside nitrate anions, and lattice water molecules. The complex is formed by two unsymmetrical tridentate ligands (L2) chelating the metal ions and forming a phenoxido-bridged Cu(II) dimer. An ORTEP view of **3** with atom-labeling scheme of the independent part is shown in Figure 4, and a selection of bond lengths and angles is given in Table 5. The metal

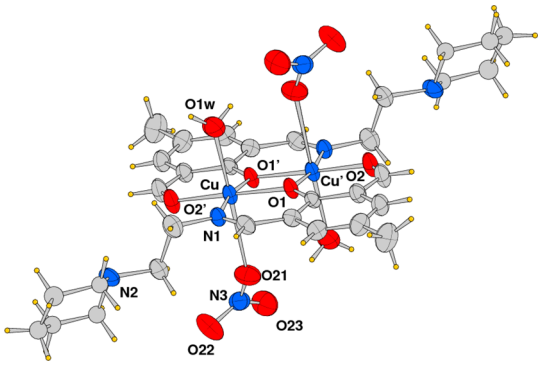

Figure 4. ORTEP drawing of the complex cation of complex **3** located on a crystallographic inversion center.

Table 5. Coordination Bond Lengths (Angstroms) and Angles (degrees) for Complex 3[a]

Cu−O(1)	1.940(4)	Cu−O(1w)	2.231(6)
Cu−O(1′)	1.951(4)	Cu−O(21)	2.582(9)
Cu−O(2′)	1.944(4)	Cu−Cu#1	3.0137(14)
Cu−N(1)	1.957(5)		
O(1)−Cu−O(2′)	170.23(19)	O(1′)−Cu−O(1w)	93.9(3)
O(1)−Cu−O(1′)	78.48(18)	N(1)−Cu−O(1w)	92.6(3)
O(2′)−Cu−O(1′)	92.30(19)	O(1)−Cu−O(21)	84.7(2)
O(1)−Cu−N(1)	93.28(18)	O(1w)−Cu−O(21)	171.5(3)
O(2′)−Cu−N(1)	95.5(2)	O(21)−Cu−N(1)	78.9(3)
O(1′)−Cu−N(1)	169.84(19)	O(21)−Cu−O(1′)	94.3(3)
O(1)−Cu−O(1w)	94.7(3)	O(21)−Cu−O(2′)	92.9(3)
O(2′)−Cu−O(1w)	89.1(3)		

[a]Primed atoms at #1 $-x + 1$, $-y$, $-z + 1$.

possesses an octahedral coordination sphere with two phenoxido-bridged oxygens, an imine nitrogen donor, and a carbonyl oxygen located in the equatorial plane and an aqua and a nitrate oxygen occupying the axial positions at longer distances. The Cu−N and Cu−O bond distances are comparable to those reported for the complexes containing the symmetric ligand L1 and one ligand ranging from 1.940(4) to 1.957(4) Å. The axial distances are significantly elongated for the Jahn−Teller effect, the Cu−O(1w) bond length, 2.231(6) Å, is significantly shorter than that involving the nitrate oxygen (Cu−O(4) 2.582(9) Å). The bond angle Cu−O1−Cu′ (101.52(18)°) leads to an intermetallic separation of 3.0137(14) Å, which is ca. 0.1 Å longer with respect to the values measured in the other complexes here reported. The piperidine moieties, in the usual chair conformation, are far apart from the metal centers with the alkyl chain in an anti periplanar conformation (torsion angle N1−C−C−N2 = 168.5(6)°).

From the above structural description of the complexes it is evident that in a few cases the X-ray data suffers from disorder. Our all efforts to get high-quality crystals on those cases failed, and we were unsuccessful to resolve the issue. However, despite the relatively poor figures of merit in some cases, which makes the absolute values of the metrical parameters for them somewhat inaccurate, the relative positions of the atoms within

dx.doi.org/10.1021/ic5005177 | Inorg. Chem. 2014, 53, 8257−8269

Table 6. Electrochemical Data of Complexes 1−15 in DMSO Medium

		DPV data E_{pc}/V	
complex	CV data[a] E^0/V or E_{pc}/V	Cu(II)/Cu(I)	Cu(I)/Cu(0)
1	0.08 (178), −0.56 (E_{pc})	0.06	−0.42
2	0.04(175), −0.51(212)	0.02	−0.44, −0.48
3	0.33(210), −0.56 (E_{pc}), −0.81 (E_{pc})	0.30, 0.15	−0.44, −0.70
4	0.06(230), −0.41(140)	0.08	−0.37
5	0.06(98)	0.22,[b] 0.08	−0.40, −0.46
6	0(320), −0.45 (E_{pc}), −1.26 (E_{pc})	0.28,[b] 0.10, −0.06	−0.36
7	0.14(100)[b], −0.31 (E_{pc}), −0.63(240)	0.19,[b] −0.16	−0.63
8	0.07(165), −0.47 (230)	0.08, −0.06	−0.46
9	0.11(106), −0.67 (E_{pc}), −0.95 (E_{pc})	0.13	−0.48, −0.83
10	0.09(183), −0.49	0.10	−0.33
11	0.05(140), −0.49 (E_{pc})	0.07	−0.33, −0.42
12	0.04 (230), −0.42(180)	0.04	−0.41
13	−0.06(320), −0.55 (E_{pc})	0.23[b], 0.06, −0.11	−0.45
14	−0.75 (E_{pc})		−0.50
15	0.06(230), −0.45	0.07	−0.40

[a]Error range: ± 0.005 V. [b]Peaks are probably due to some unidentified degradation product.

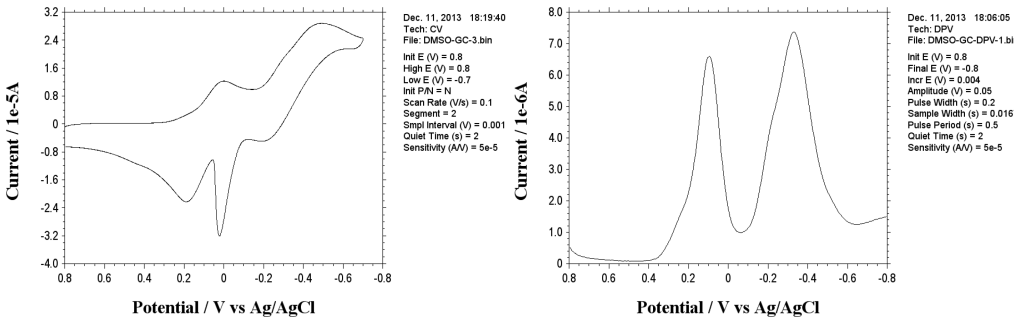

Figure 5. CV and DPV spectrum of complex **10** at the GC electrode at 100 mV s^{-1} scan rate as representative.

these complexes are sufficiently accurate to describe the shape of these molecules.

Electrochemistry of the Complexes. The redox behavior of the complexes was explored using cyclic voltammetry (CV) and differential pulse voltammetry (DPV), and the data is tabulated in Table 6. The CV and DPV pictures of complex **10** are presented in Figure 5 as a representative one, and some other representative voltammograms are given in the Supporting Information (Figures S14−S17). The Cu(II)/Cu(I) couple appears near 0.0 V with respect to the Ag/AgCl electrode, and in most cases in the CV experiments the two Cu(II)/Cu(I) couples are not resolved, though in DPV these two couples are sometimes resolved. It has been argued that DPV is a very good technique for resolving redox responses having small differences in peak potentials, provided the two peaks differ in their formal potential by more than 180 mV.[33] The fact that in our case we were unable to resolve the two Cu(II)/Cu(I) couples for most of the compounds by CV or DPV experiments suggests that the formal potentials for the two successive metal reductions differ by less than 180 mV, and hence, the mixed-valent $Cu^{I}Cu^{II}$ species will be unstable. Thus, during the catalytic cycle involving two-electron oxidation of catechol a one-electron redox intermediate is disfavored. The reductive process at around −0.4 V is assigned to Cu(I)/Cu(0) reduction as after cycling through the potential a strong stripping current is observed in the reverse (anodic) scan in CV experiments.[11] In CV experiments the Cu(II)/Cu(I) couple(s) appears either as quasi-reversible, with a relatively high ΔE_p value ($\Delta E_p = E_{pa} - E_{pc}$), or in few cases as an irreversible reduction redox process with $i_{pc}/i_{pa} \ll 1$, which is typical of Cu(II)/Cu(I) reduction in many of its complexes.[10,11,20] It has been argued that though the formal potential ($E^{\circ\prime}$) is equal to the mid peak potential ($E_{pa} + E_{pc}$)/2 determined by cyclic voltammetry, and this relationship is strictly valid for ideal reversible couples; for quasi-reversible systems the mid peak potential may also be used as the formal potential. This is because for quasi-reversible systems the amount of shift of the cathodic peak toward more negative potential values is compensated by an almost equal shift of the reoxidation peak toward more positive values.[33] Thus, in our case also we assumed the mid peak potential in CV experiments is very close to the formal potential ($E^{\circ\prime}$). In fact, from Table 6 it can be seen that the DPV peak potentials are very close to the $E^{\circ\prime}$ value obtained from CV experiments. As in our case DPV peak potentials can be more accurately measured than that of CV peaks, we have taken the DPV peak potentials for our attempted correlation study with the k_{cat} values. Where the two Cu(II)/Cu(I) potentials were observed in DPV we have taken an average value of the two potentials for correlation purpose.

For each complex it is expected that the Cu(II)/Cu(I) reduction potentials should follow the order of Hammett σ_p values of the substituent on the diformyl phenyl ring; a more positive σ_p value (meaning more electron withdrawing character) should lead to more positive Cu(II)/Cu(I) potential. σ_p values for Cl, ^{t}Bu, and Me groups are 0.227, −0.151, and

dx.doi.org/10.1021/ic5005177 | Inorg. Chem. 2014, 53, 8257−8269

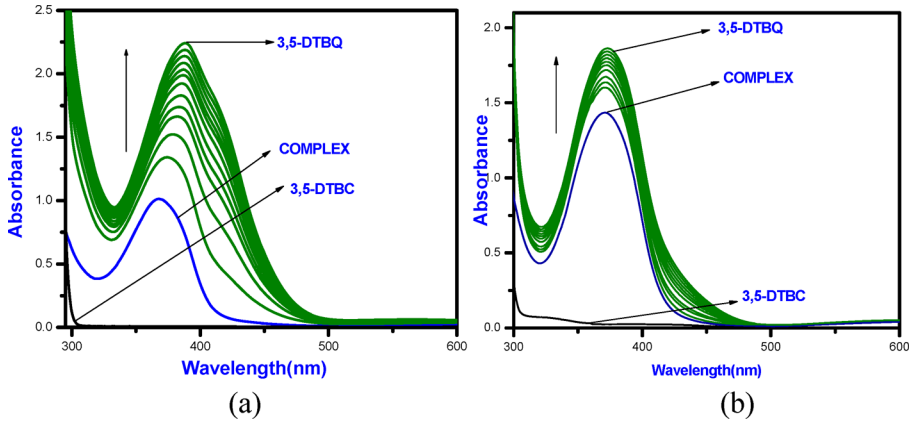

Figure 6. Changes observed in UV−vis spectra of complexes (a) **2** and (b) **14** (conc. 1×10^{-4} M) upon addition of 100-fold 3,5-DTBC (1×10^{-2} M) in DMSO medium.

−0.170, respectively,[34] and the Cu(II)/Cu(I) potential is expected to be most positive for the chloro derivatives. On the other hand, the σ_p values for ^{t}Bu and Me are very comparable (a very small difference of ca. 0.02), so it is expected that these groups affect the potentials at a comparable degree and any difference between them will be largely determined by steric factors. This expected trend was found to be confirmed by complexes with six ligands L1[5], L1[6], L2[3], L1[10], L1[12], and H_2L1[11], namely, complexes **6**, **7**, **13**, **10**, **11**, and **15**, respectively. In the case of complexes **1**, **2**, and **3** derived from three different ligands, namely, L1[1], L1[2], and L21, the Cl-substituted compound (complex **1**) has an expectedly higher $E°$ value than the ^{t}Bu-substituted compound **2**; however, the Me-substituted compound **3** has much higher $E°$ value than even the Cl-substituted compound **1**, and this may be due to the different structure of the Me compound (complex **3**). The electrochemical behavior of complexes **4**, **5**, and **12** is anomalous. Complex **5** having a ^{t}Bu substituent gives the most positive $E°$ value, whereas $E°$ values of complex **4** (having a Cl substituent) and complex **12** (having a Me substituent) are very comparable. Among complex **8**, **9**, and **14** again the ^{t}Bu substituent (complex **9**) gives a higher $E°$ value than the chloro species (complex **8**); for the Me-substituent complex **12** of this series the Cu(II)/Cu(I) couple could not be detected.

It is expected that complexes **6**, **7**, and **13** having a propyl group in the ligand backbone should show more facile Cu(II)/Cu(I) reduction (more positive $E°$ value) compared to the analogous complexes **4**, **5**, and **12**, respectively, having an ethyl group in the ligand backbone, because of their greater steric flexibility, which allows structural rearrangement on electron transfer. This is indeed the case for the chloro (complexes **4** and **6**) and methyl (complexes **13** and **12**) series of compounds, but this trend is not observed for ^{t}Bu series, where compound **5** has an abnormally high positive value of the Cu(II)/Cu(I) potential compared to the other two compounds of that series.

Thus, the results discussed above indicate that the R group at the para position affects the electrochemical property of the complexes, although in some cases the relationship is not unambiguously interpreted.

It is worth noting that when the binuclear Cu(II) complexes were reacted with 3,5-DTBC, two new peaks at 0.3−0.4 and 0.1−0.2 V were detected in DPV experiments. It has been reported that Cu^{II}(bpy)(DTBC) and Cu^{II}(phen)(DTBC) complexes undergo a two-electron oxidation leading to DTBQ at around 0.05 V vs SCE and around 0.1 V vs Ag/AgCl. In the same potential region Cu^{II}(en)(DTBC) undergoes two successive one-electron oxidations.[35] On the basis of the above observations we assign the new peaks at 0.1−0.2 and 0.3−0.4 V to Cu(II)-bound catechol to semiquinone and semiquinone to quinone oxidations (Figure S19, Supporting Information).

Catecholase Activity. Catechol oxidase, a type-3 copper protein, can bind oxygen reversibly at room temperature, and so it can be used to oxidize phenols to the respective *o*-benzoquinones. As a model of the enzyme we have taken 15 dinuclear complexes of Cu(II) and studied their efficiency toward oxidation of 3,5-di-*tert*-butylcatechol (3,5-DTBC) to 3,5-di-*tert*-butylbenzoquinone (3,5-DTBQ). Interestingly, all of them display significant catalytic activity toward oxidation of 3,5-DTBC to 3,5-DTBQ in DMSO medium. Before proceeding into a detailed kinetic study to evaluate the ability of our complexes to mimic the active site of catechol oxidase, 1×10^{-4} mol dm^{-3} solutions of complexes **1**−**15** were treated with 1×10^{-2} mol dm^{-3} (100 equiv) of 3,5-DTBC under aerobic condition. The course of the reaction was followed by UV−vis spectroscopy (Figures S20−S32, Supporting Information). The time-dependent UV−vis spectral scan was performed in pure DMSO medium. All complexes behave similarly, showing a smooth conversion of 3,5-DTBC to 3,5-DTBQ. Figure 6a and 6b shows the spectral change for **2** (as representative of *tert*-butyl complexes) and **14** (as representative of methyl complexes) upon addition of 100-fold 3,5-DTBC (1×10^{-2} M) observed at an interval of 5 min in DMSO medium. The kinetics of the 3,5-DTBC oxidation was determined by monitoring the increase of the product 3,5-DTBQ. The experimental conditions were the same as we reported earlier using ε of 3,5-DTBQ in DMSO = 2100 M^{-1} cm^{-1}.[18] All complexes showed saturation kinetics, and a treatment based on the Michaelis−Menten model seemed to be appropriate. The binding constant (K_M), maximum velocity (V_{max}), and rate constant for dissociation of substrates (i.e., turnover number, k_{cat}) were calculated for all complexes using the Lineweaver−Burk graph of $1/V$ vs $1/[S]$ (Figures S33−S62, Supporting Information) using the eq $1/V = \{K_M/V_{max}\}\{1/[S]\} + 1/V_{max}$. The calculated values of the kinetic parameters V_{max} ranges from 7.483×10^{-7} to 6.858×10^{-6} (standard deviation ranges $\pm 0.0001 \times 10^{-6}$ to $\pm 0.133 \times 10^{-6}$), K_M ranges from 1.918×10^{-2} to 7.898×10^{-4} (standard deviation ranges $\pm 0.02 \times 10^{-3}$ to $\pm 0.404 \times 10^{-3}$), and k_{cat} ranges from 0.501×10^{2} to $2.468 \times$

dx.doi.org/10.1021/ic5005177 | Inorg. Chem. 2014, 53, 8257−8269

10^2 (standard deviation ranges from 0.00009 × 10^2 to 0.09 × 10^2).

Data from Table 7 indicate that the group at the para position has a significant high impact on the catecholase activity, and the k_{cat} values for complexes containing L1[3], L1[4], and HL2[2] ligands (namely, complexes **4**, **5**, and **12**), L1[5], L1[6], and L2[3] ligands (namely, complexes **6**, **7**, and **13**) and L1[10], L1[12], and H_2L1[11] ligands (namely, complexes **10**, **11**, and **15**) follow the influence of R groups in the order chloro > methyl > *t*-butyl, in accord with the electron-withdrawing property, i.e., complexes with the most electron-withdrawing chloro group show the highest activity and vice versa. However, a similar trend is not observed in other cases.

Table 7. k_{cat} Values for the 15 Dinuclear Complexes

complex	$k_{cat} \times 10^2$ (in h^{-1})	complex	$k_{cat} \times 10^2$ (in h^{-1})
1	0.737	**9**	0.518
2	0.505	**10**	0.683
3	0.846	**11**	0.501
4	1.272	**12**	0.907
5	0.496	**13**	0.546
6	2.468	**14**	1.178
7	0.507	**15**	0.542
8	0.269		

Correlation between k_{cat} and Electrochemical Property of the Complexes. In 1997, Krebs et al., one of the pioneers of catechol oxidase model study, tried to establish a correlation between catecholase activity and electrochemical property of a series of dicopper(II) complexes of phenol-based Mannich ligands. However, they failed to find any clear relationship between the electrochemical properties and the catecholase activity of the complexes. In addition, they stated that the poorly defined redox chemistry of that class of complexes would never allow one to establish such a correlation. In 2002, Belle and co-workers tried to evaluate the effect of the para substituent groups of a ligand system similar to that of Krebs on the catecholase activity and on the electrochemical property of their dicopper(II) complexes. They observed that the catalytic properties of their complexes depend on the electronic effects reflected by their redox potential values, even though the electronic effects did not control solely the reactivity. Here again we are trying to unfold the effect of the substituent groups in the para position of the bridging phenolate group on catecholase and on the electronic property of dicopper(II) complexes. Belle et al. reported that the strongly electron-withdrawing trifluoromethyl group completely inhibits the activity, the poorly electron-withdrawing fluorine atom inhibits to a moderate extent, and the strongly electron-donating methoxyl group increases notably the activity. On the contrary, here we observed that the activity remarkably increases with the electron-withdrawing chloro group whereas it decreases with the electron-donating *tert*-butyl group considering the corresponding complex with a methyl at the para position as a reference especially for nine complexes, namely, complexes **4**, **5**, and **12**, complexes **6**, **7**, and **13**, and complexes **10**, **11**, and **15**. Among the several possibilities, (i) enzyme−substrate adduct formation and (ii) reduction of Cu(II) to Cu(I) are the possible rate-determining steps. If the former is the key step in catalysis the effect of electrochemical property changes on changing the para substituent groups should not be prominent on catecholase activity. Belle and co-workers explained their observed effect on considering enzyme−substrate adduct formation as the key step in their catalysis. On the other hand, our observation clearly suggests that possibility (ii) should be the key step in our catalysis, especially with complexes **6**, **7**, and **13**, omplexes **10**, **11**, and

Scheme 3. Catalytic Cycle of Catechol Oxidation by a Generic Dicopper Complex Used in This Study[a]

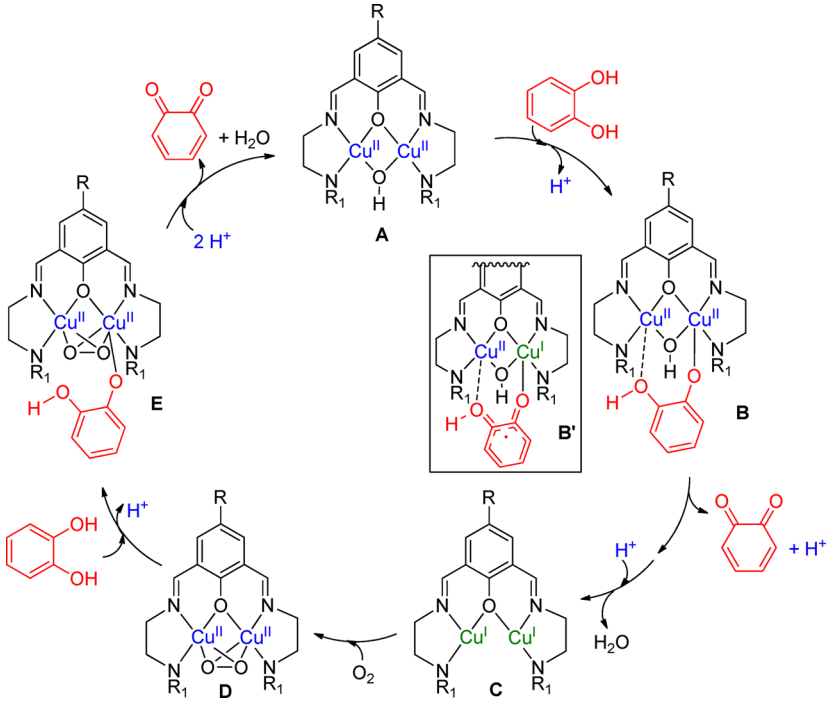

[a]Two molecules of catechol are oxidized coupled with the reduction of molecular oxygen to water.

dx.doi.org/10.1021/ic5005177 | Inorg. Chem. 2014, 53, 8257−8269

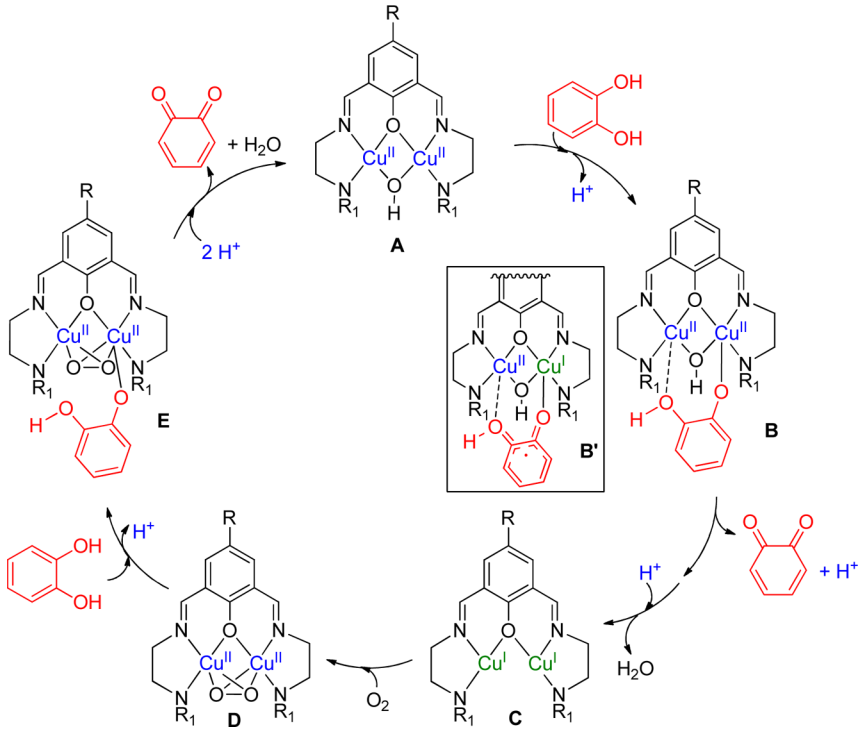

Figure 7. BP86/def2-TZVP-optimized structures of **A**–**E** intermediates of the catalytic cycle. Distances in Angstroms. Hydrogen atoms have been omitted for clarity apart from the OH group of the coordinated catechol to differentiate it from the anionic oxygen atom.

15, and complexes **8**, **9**, and **14** series, and therefore, we are supposed to get a better correlation between electrochemical property and catecholase activity in those cases. On comparing Tables 6 and 7 another interesting point may be stated that the E° value is proportional to the k_{cat} value for certain ligand series complexes, e.g., complexes **1**–**3** and complexes **8** and **9**. However, in other cases we cannot see any direct relation between the electrochemical property and the catecholase activity of the complexes, and the reason is not at all clear to us at this moment. However, Neves et al. in one of their classical works tried to establish a relation between the kinetic parameters and the electrochemical properties. They observed a very good relation between kinetic parameter k_2 (second-order rate constant = k_{cat}/K_M) and $(\Delta E)_{1,2}$ $(=E(\text{red})_1 - E(\text{red})_2)$, although no good correlation was noticed between k_{cat} and E°.

Theoretical Study. From the above discussion it is clear that we do not get a very linear relationship between E° and k_{cat} all the time. As stated earlier, redox participation of two copper centers appears to be crucial in catecholase activity. Thus, we do believe that the k_{cat} value should be related to a certain factor associated with electrochemical change of the catalyst in the catalytic cycle, and that very idea prompted us to perform a detailed DFT theoretical study especially on the reaction pathway involved in this catalysis. It should be mentioned that the E° values are computed in the original complexes, and the reduction of Cu(II) to Cu(I) in the catalytic cycle occurs in a species where the catechol is coordinated to the complex; consequently, the E° value of this species may differ considerably from that of the uncoordinated complex. To perform the theoretical study we used the catalytic cycle proposed by Krebs and co-workers[36] and redrawn by Reedijk and co-workers.[37] We observed in the optimized catechol complexes an ancillary interaction between the phenolic group of catechol and one copper metal center, and we indicated this interaction as a dashed line (see **B** complex in Scheme 3). We focused our study in the first part of the mechanism, i.e., from the met state (**A**) to the deoxy state (**C**) and subsequent oxidation to **D**. We studied a possible correlation between the energy associated with each step and the experimental k_{cat} values. We optimized compounds **A**, **B**, and **C** for the Cl and Me series of complexes in order to see differences between an electron-withdrawing and electron-donating substituent. Since formation of the catechol complex (**B**) is energetically favorable for all complexes it is expected to be a fast step of the mechanism. In contrast, conversion of compound **B** to **C** is unfavorable energetically because both Cu ions are reduced and the coordinated ligands are released (oxidized catechol and a water molecule). Experimental observations (vide supra) suggest that oxidation of 3,5-DTBC is produced via two steps, semibenzoquinone followed by quinone formation with concomitant reduction of Cu(II) to Cu(I). Therefore, conversion of **B** to **C** is likely formed by two consecutive one-electron transfer reactions with formation of an intermediate denoted as **B′** in Scheme 3. We computed the energetic cost of this process for two series of complexes (R = Cl and Me) in order to investigate if there is a correlation between the energetic cost of this step and the catalytic constant. We have not performed the study for the R = ^{t}Bu series because four out of five complexes present very similar $k_{cat} \approx 50\ h^{-1}$, and consequently, it was impracticable to correlate the data.

In Figure 7 we represent the optimized geometries for L^3 (R = Cl) complexes **A**–**E**, as an exemplifying model system. It can be observed that the monocoordinated catechol molecule forms the aforementioned ancillary interaction with the other copper metal center (Cu–OH distance 2.61 Å). This interaction is important to fix the final geometry of the catechol in the

dx.doi.org/10.1021/ic5005177 | Inorg. Chem. 2014, 53, 8257–8269

complex and likely facilitates the electron transfer from the catechol to the Cu(II) ions. It is interesting to note the optimized geometry of compound **D**, where the copper ions have been reoxidized, the O−O distance is 1.42 Å, and all Cu−O distances are very similar, ranging from 2.11 to 2.13 Å. We also studied the subsequent complexation of catechol to form complex **E**. The global transformation of **C** to **E** that involves incorporation of molecular oxygen, oxidation of the Cu(I) ions, and complexation of catechol is energetically very favorable (−68.9 kcal/mol) for the system shown in Figure 8.

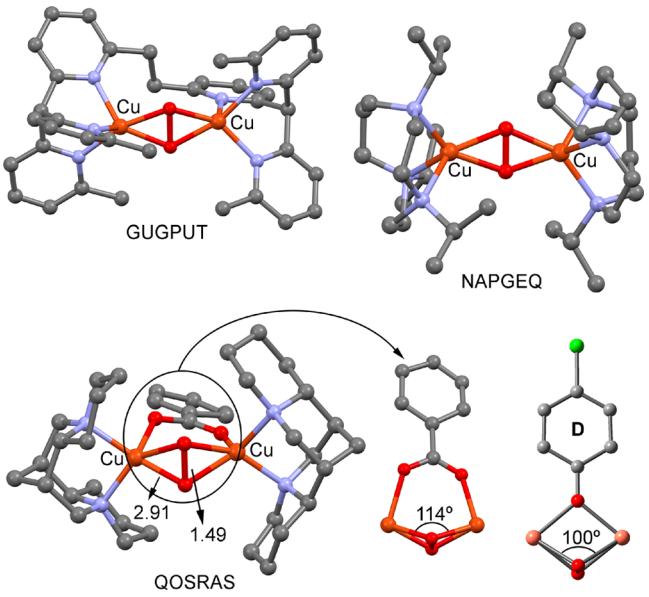

Figure 8. Partial views of the X-ray structures of GUGPUT, NAPGEQ, QOSRAS, and the optimized intermediate **D** for comparison purposes. Hydrogen atoms have been omitted for clarity. Distances in Angstroms.

It should be mentioned that we studied theoretically and experimentally other orientations and conformations for the intermediate **D**. In Figure S63, Supporting Information, we show three different orientations that we studied in combination to searches in the Cambridge Structural Database (CSD) to give experimental support to the DFT calculations. In Figure 8 we show several X-ray structures that exhibit the coordination mode of O_2 proposed in the intermediate **D**. In particular, (μ^2-(1,2-bis(2-(bis(6-methyl-2-pyridyl)methyl)-6-pyridyl)ethane-*N*,*N*′,N″))-(μ^2-peroxo)-dicopper (GUGPUT)[38] and (μ^2-peroxo)-bis(1,4,7-tris(isopropyl)-1,4,7-triazacyclodecane)-dicopper (NAPGEQ)[39] structures do not present additional oxo-bridging ligands in the structure. Conversely, it is remarkable that the geometry of the (μ^2-benzoato)-(μ^2-peroxo)-bis(α-isosparteine)-dicopper (QOSRAS)[40] structure is similar to the optimized geometry of intermediate **D** (see Figure 8, bottom right) concerning bond distances and angles, keeping in mind that the two copper centers are bridged by a carboxylate instead of phenolate (the Cu−O_2 unit is less butterfly distorted).

We also analyzed the spin density and single-occupied molecular orbitals (SOMOs) of intermediate **B**′ that are shown in Figure 9. In this electronic configuration one electron has been transferred from the catechol to one metal center. The spin density plot simply reflects the sum of both SOMOs, and it can be clearly observed that some spin density is delocalized

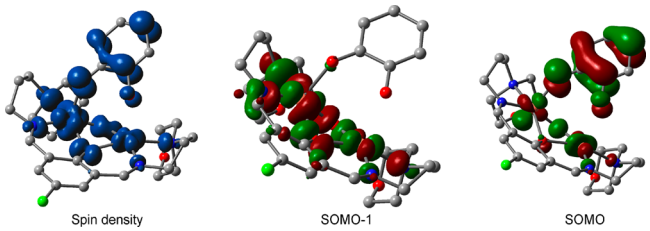

Figure 9. Spin density (left) and SOMOs of intermediate **B**′.

onto the atoms of the ligands directly bonded to the metal centers and the catechol ring. The SOMO shows the contribution of the π system of the semiquinonate moiety to this orbital with partial contribution of the d atomic orbitals of the metal centers. In contrast, the catechol does not participate in the SOMO-1, which has the contribution of the atomic orbitals of the metal centers and the atoms directly bonded to them.

In Table 8 we summarize the energetic cost on going from intermediate **B** to **C** for the R = Cl and R = Me series and the

Table 8. Reaction Energy Necessary for Conversion of B to C

complex	ΔE (kcal/mol)	ΔE_{rel} (kcal/mol)	$k_{cat} \times 10^2$ (h^{-1})
1	38.2	11.3	0.7372
3	42.3	4.6	0.8451
4	36.1	9.2	1.272
6	26.9	0.0	2.45
8	42.1	15.1	0.2690
10	39.5	12.6	0.6827
12	39.2	1.6	0.9090
13	40.4	2.8	0.754
14	37.6	0.0	1.1681
15	46.7	9.0	0.5421

experimental catalytic constant values for comparison purposes. For each series we also included the relative energies with respect to the most favorable conversion. It should be mentioned that the energies have been computed taking into account solvation effects by means of a continuum model. As aforementioned, this process is unfavorable due to the loss of two coordinating ligands in this mechanistic step. We are interested in the variation of the energy required to oxidize catechol and concomitant reduction of Cu(II) to Cu(I) depending on the substituents of the ligands. We represented in Figure 10 the relative energy values versus the experimental k_{cat} values resulting in interesting correlations. As it can be observed we found a very good correlation between the relative energy and k_{cat} (R = 0.995) for the R = Cl series that strongly support the hypothesis that the key mechanistic step is the reduction of Cu(II) to Cu(I). It is worth mentioning that such correlation is not obtained using the experimental E° reduction potential values. This likely indicates that the coordination of the catechol to the complex influences the reduction ability of the copper ions due to a combination of the coordination itself and steric effects. The same representation for the R = Me series also shows a rather good correlation between the relative energy and the experimental k_{cat} values (R = 0.903). If both series are gathered in the same representation the regression coefficient is also good (R = 0.912), which further confirms that there is a clear correlation between the k_{cat} values and the Cu(II) to Cu(I) reduction, which does not necessarily

dx.doi.org/10.1021/ic5005177 | *Inorg. Chem.* 2014, 53, 8257−8269

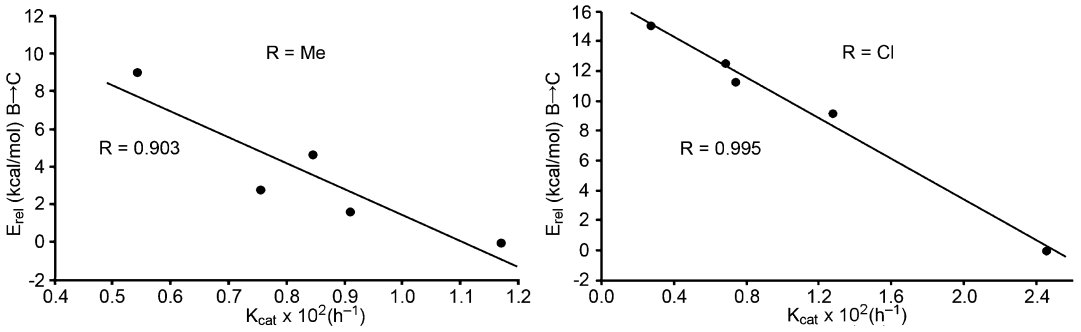

Figure 10. Regression plots of k_{cat} versus the relative energy cost for conversion of **B** to **C** (see Scheme 3).

correspond to the electrochemical properties of the free complexes.

CONCLUSIONS

In order to explore the deep insight on the correlation between the electrochemical behavior and the catecholase activity of synthetic analogues of catechol oxidase, a nearly unanswered corner of catecholase activity, we designed and synthesized 15 closely related dicopper(II) complexes of phenol-based compartmental ligands. Eleven of them are newly introduced, and four were reported earlier. The 11 new complexes have been characterized by routine physicochemical techniques, and complexes **1**−**3** and **8**−**10** have further been structurally characterized by X-ray single-crystal structural analyses. Electrochemical and catecholase activities of all complexes have been thoroughly investigated in DMSO medium. CV and DPV analyses reveal that oxidation of 3,5-DTBC catalyzed by dicopper(II) complexes proceed via two steps: first semibenzoquinone followed by benzoquinone with concomitant reduction of Cu^{II} to Cu^{I}. Our critical analysis reveals that apparently there is nearly no linear relationship between k_{cat} and E° values of the complexes. That very observation prompted us to calculate the energetics associated with each step of the catalysis, and interestingly, we were successful to establish for the first time quite a good linear relationship between the energetic cost for the catechol-bound Cu^{II} to Cu^{I} reduction and k_{cat} values.

ASSOCIATED CONTENT

Supporting Information

X-ray crystallographic data in CIF format of complexes **1**−**3** and **8**−**10**, FT-IR spectra, wavelength scans for catecholase activity, kinetic plots, ORTEP views of complexes **2** and **10**, cyclic voltammograms, and differential pulse voltammograms. This material is available free of charge via the Internet at http://pubs.acs.org.

AUTHOR INFORMATION

Corresponding Authors

*E-mail: shyamalchattopadhyay@gmail.com.
*E-mail: toni.frontera@uib.es.
*E-mail: ezandgando@units.it.
*E-mail: dasdebasis2001@yahoo.com .

Notes

The authors declare no competing financial interest.

ACKNOWLEDGMENTS

The authors thank CSIR, New Delhi [01(2464)/11/EMR-II dt 16-05-11 to DD], for financial support and the University of Calcutta for providing the facility of the single-crystal X-ray diffractometer from the DST FIST program. A.B. and A.F. acknowledge the Spanish Ministerio de Economía y Competitividad (MINECO) (Projects, and CONSOLIDER INGENIO 2010, CSD2010-00065, FEDER funds) and the Direcció General de Recerca i Innovació del Govern Balear (project 23/2011, FEDER funds) for financial support. We thank the CTI (UIB) for computational facilities. This paper is dedicated to the memory of Pali Maiti, whom we lost very untimely and unfortunately.

REFERENCES

(1) (a) Eicken, C.; Zippel, F.; Buldt-Karentzopoulos, K.; Krebs, B. *FEBS Lett.* **1998**, *436*, 293. (b) Than, R.; Feldmann, A. A.; Krebs, B. *Coord. Chem. Rev.* **1999**, *182*, 211. (c) Gentschev, P.; M?ller, N.; Krebs, B. *Inorg. Chim. Acta* **2000**, *300*, 442. (d) Merkel, M.; Mçller, N.; Piacenza, M.; Grimme, S.; Rompel, A.; Krebs, B. *Chem.—Eur. J.* **2005**, *11*, 1201.

(2) Monzani, E.; Quinti, L.; Perotti, A.; Casella, L.; Gullotti, M.; Randaccio, L.; Geremia, S.; Nardin, G.; Faleschini, P.; Tabbi, G. *Inorg. Chem.* **1998**, *37*, 553.

(3) Manzur, J.; Garcia, A. M.; Vega, A.; Spodine, E. *Polyhedron* **1999**, *18*, 2399.

(4) (a) Torelli, S.; Belle, C.; Gautier-Luneau, I.; Pierre, J. L.; Saint-Aman, E.; Latour, J. M.; Le Pape, L.; Luneau, D. *Inorg. Chem.* **2000**, *39*, 3526. (b) Belle, C.; Selmeczi, K.; Torelli, S.; Pierre, J.-L. *C. R. Chim.* **2007**, *10*, 271.

(5) Gupta, M.; Mathur, P.; Butcher, R. J. *Inorg. Chem.* **2001**, *40*, 878.

(6) Murthy, N. N.; Mahroof-Tahir, M.; Karlin, K. D. *Inorg. Chem.* **2001**, *40*, 628.

(7) Kao, C. H.; Wei, H. H.; Liu, Y. H.; Lee, G. H.; Wang, Y.; Lee, C. J. *J. Inorg. Biochem.* **2001**, *84*, 171.

(8) Fernandes, C.; Neves, A.; Bortoluzzi, A. J.; Mangrich, A. S.; Rentschler, E.; Szpoganicz, B.; Schwingel, E. *Inorg. Chim. Acta* **2001**, *320*, 12.

(9) Mukherjee, J.; Mukherjee, R. *Inorg. Chim. Acta* **2002**, *337*, 429.

(10) Neves, A.; Rossi, L. M.; Bortoluzzi, A. J.; Szpoganicz, B.; Wiezbicki, C.; Schwingel, E.; Haase, W.; Ostrovsky, S. *Inorg. Chem.* **2002**, *41*, 1788.

(11) (a) Ackermann, J.; Meyer, F.; Kaifer, E.; Pritzkow, H. *Chem.—Eur. J.* **2002**, *8*, 247. (b) Ackermann, J.; Buchler, S.; Meyer, F. *C. R. Chim.* **2007**, *10*, 421.

(12) Seneque, O.; Campion, M.; Douziech, B.; Giorgi, M.; Riviere, E.; Journaux, Y.; Mest, Y. L.; Reinaud, O. *Eur. J. Inorg. Chem.* **2002**, 2007.

(13) (a) Koval, I. A.; Pursche, D.; Stassen, A. F.; Gamez, P.; Krebs, B.; Reedjik, J. *Eur. J. Inorg. Chem.* **2003**, 1669. (b) Koval, I. A.; Huisman, M.; Stassen, A. F.; Gamez, P.; Lutz, M.; Spek, A. L.; Reedijk, J. *Eur. J. Inorg. Chem.* **2004**, 591.

(14) Sreenivasulu, B.; Vetrichelvan, M.; Zhao, F.; Gao, S.; Vittal, J. J. *Eur. J. Inorg. Chem.* **2005**, 4635.
(15) Wegner, R.; Gottschaldt, M.; Wolfgang, P.; Jager, E.-G.; Klemm, D. *J. Mol. Catal. A* **2003**, *201*, 93.
(16) Thirumavalavan, M.; Akilan, P.; Kandaswamy, M.; Chinnakali, K.; Kumar, G. S.; Fun, H. K. *Inorg. Chem.* **2003**, *42*, 3308.
(17) Kaizer, J.; Csonka, R.; Speir, G.; Giorgi, M.; Reglier, M. *J. Mol. Catal. A* **2005**, *235*, 81.
(18) Banu, K. S.; Chattopadhyay, T.; Banerjee, A.; Bhattacharya, S.; Suresh, E.; Nethaji, M.; Zangrando, E.; Das, D. *Inorg. Chem.* **2008**, *47*, 7083.
(19) (a) Guha, A.; Chattopadhyay, T.; Paul, N. D.; Mukherjee, M.; Goswami, S.; Mondal, T. K.; Zangrando, E.; Das, D. *Inorg. Chem.* **2012**, *51*, 8750. (b) Adhikary, J.; Chakraborty, P.; Das, S.; Chattopadhyay, T.; Bauza, A.; Chattopadhyay, S. K.; Ghosh, B.; Mautner, F. A.; Frontera, A.; Das, D. *Inorg. Chem.* **2013**, *52*, 13442. (c) Ghosh, T.; Adhikary, J.; Chakraborty, P.; Sukul, P. K.; Jana, M. S.; Mondal, T. K.; Zangrando, E.; Das, D. *Dalton Trans.* **2014**, *43*, 841.
(20) Reim, J.; Krebs, B. *J. Chem. Soc., Dalton Trans.* **1997**, 3793.
(21) Torelli, S.; Belle, C.; Hamman, S.; Pierre, J.-L. *Inorg. Chem.* **2002**, *41*, 3983.
(22) Meiwes, D.; Ross, B.; Kiesshauer, M.; Cammann, K.; Witzel, H.; Knoll, M.; Borchardt, M.; Sandermaier, C. *Lab. Med.* **1992**, *15*, 24.
(23) Sreenivasulu, B.; Zhao, F.; Gao, S.; Vittal, J. J. *Eur. J. Inorg. Chem.* **2006**, 2656.
(24) Saha, S.; Koner, S.; Tuchagues, J.-P.; Boudalis, A. K.; Okamoto, K.-I.; Banerjee, S.; Mal, D. *Inorg. Chem.* **2005**, *44*, 6379.
(25) Gagne, R. R.; Spiro, C. L.; Smith, T. J.; Hamann, C. A.; Thies, W. R.; Shiemeke, A. K. *J. Am. Chem. Soc.* **1981**, *103*, 4073.
(26) *SMART, SAINT, Software Reference Manual*; Bruker AXS Inc.: Madison, WI, 2000.
(27) Sheldrick, G. M. *Acta Crystallogr.* **2008**, *64*, 112.
(28) Farrugia, L. J. *J. Appl. Crystallogr.* **2012**, *45*, 849.
(29) Ahlrichs, R.; Bar, M.; Hacer, M.; Horn, H.; Komel, C. *Chem.Phys.Lett.* **1989**, *162*, 165.
(30) Klamt, A.; Schuurmann, G. *J. Chem. Soc., Perkin Trans. 2* **1993**, 799.
(31) Nakamoto, K. *Infrared and Raman Spectra of Inorganic and Coordination Compounds*, 3rd ed.; Wiley: New York, 1978.
(32) Lever, A. B. P. *Inorganic Electronic Spectroscopy*; Elsevier: Amsterdam, The Netherlands, 1984; p 553.
(33) (a) *Zanello, Inorganic Electrochemistry: Theory, Practice and Applications*; The Royal society of Chemistry, U. K., 2003; pp110–113. (b) Richardson, D. E.; Taube, H. *Inorg. Chem.* **1981**, *20*, 1278.
(34) McDaniel, D. H.; Brown, H. C. *J. Org. Chem.* **1958**, *23*, 420.
(35) Harmalker, S.; Jones, S. E.; Sawyer, D. T. *Inorg. Chem.* **1983**, *22*, 2790.
(36) Gerdemann, C.; Eicken, C.; Krebs, B. *Acc. Chem. Res.* **2002**, *35*, 183.
(37) Koval, I. A.; Belle, C.; Selmeczi, K.; Philouze, C.; Saint-Aman, E.; Schuitema, A. M.; Gamez, P.; Pierre, J. L.; Reedijk, J. *J. Biol. Inorg. Chem.* **2005**, *10*, 739.
(38) Kodera, M.; Katayama, K.; Tachi, Y.; Kano, K.; Hirota, S.; Fujinami, S.; Suzuki, M. *J. Am. Chem. Soc.* **1999**, *121*, 11006.
(39) Lam, B. M. T.; Halfen, J. A.; Young Junior, V. G.; Hagadorn, J. R.; Holland, P. L.; Lledos, A.; Cucurull-Sanchez, L.; Novoa, J. J.; Alvarez, S.; Tolman, W. B. *Inorg.Chem.* **2000**, *39*, 4059.
(40) Funahashi, Y.; Nishikawa, T.; Wasada-Tsutsui, Y.; Kajita, Y.; Yamaguchi, S.; Arii, H.; Ozawa, T.; Jitsukawa, K.; Tosha, T.; Hirota, S.; Kitagawa, T.; Masuda, H. *J. Am. Chem. Soc.* **2008**, *130*, 16444.